R. & M. No. 3416

MINISTRY OF AVIATION

AERONAUTICAL RESEARCH COUNCIL
REPORTS AND MEMORANDA

An Investigation of the Flow about Circular Cylinders Placed Normal to a Low-Density, Supersonic Stream

By S. C. METCALF, C. J. BERRY and MISS B. M. DAVIS

LONDON: HER MAJESTY'S STATIONERY OFFICE
1965
PRICE 13*s.* 6*d.* NET

An Investigation of the Flow about Circular Cylinders Placed Normal to a Low-Density, Supersonic Stream

By S. C. METCALF, C. J. BERRY and MISS B. M. DAVIS

*Reports and Memoranda No. 3416**

April, 1964

Summary.

The pressure distribution around circular cylinders has been measured near $M_\infty = 2$, for Reynolds numbers between 5 and 135. The induced pressure due to viscous effects has been estimated using a 'tangent-cylinder' method and found to agree well with experiment. The pressure drag is shown to increase gradually with rarefaction, and the estimated skin-friction drag increased as $1{\cdot}7/\sqrt{Re_D}$. A diagram of the flow has been built up from the pressure measurements, wake traverses, and argon-afterglow photographs.

LIST OF CONTENTS

* Replaces N.P.L. Aero. Report No. 1097—A.R.C. 25 793.

Published with the permission of the Director, National Physical Laboratory.

1. *Introduction.*

The present interest in very high-altitude flight where the air density is extremely low poses many problems seldom encountered in high-Reynolds-number continuum flow. One of the more important of these is the influence of the thick laminar boundary layers surrounding the body. These thick boundary layers, which are characteristic of low-density flows, induce pressure changes on the body surface, modify the position and extent of flow separation, and also are responsible for an increasingly large skin-friction drag.

The study of rarefied gas flows, between the limits of continuum and free-molecular flow is at present severely hampered by the lack of an overall solution of the Boltzmann equation for an arbitrary gas density. To overcome this handicap it is necessary to build up a general picture of rarefied flow in this particular range of conditions from experimental data. For this purpose several low-density wind tunnels have been built, including one at the N.P.L.

It was the object of the present experiment to provide information on the influence of the boundary layer developing about a circular cylinder in low-density flow, by making detailed measurements of the surface pressures. By comparing these pressure distributions with known high-Reynolds-number results for a similar body and at about the same stream Mach number, it was hoped that the induced, viscous effects could be assessed. Moreover, some insight might be gained into the nature of the near wake behind the cylinder. Because of the somewhat exploratory nature of the tests the emphasis has been placed on approximate estimations of viscous-induced pressure increments, skin-friction drag, separation point, etc. Simple, easily-computed, theories have been used where possible.

Some information on pressure distributions around circular cylinders in low-density flow is already available from the work of Tewfik and Giedt[6], but this is for smaller Knudsen numbers than the present tests (i.e. less rarefied flow) where the skin-friction drag is much less significant. Data on the total drag of circular cylinders in low-density flow obtained by Sreekanth[3] and by Maslach and Schaaf[4] may be used in conjunction with the present results to estimate the skin-friction drag at small Reynolds numbers.

Experiments in the transition-flow régime have a handicap in the lack of efficient, sensitive flow-visualisation systems. The argon-afterglow technique used in the present tests gives some indication of the gross flow characteristics, but such information was supplemented by pitot-pressure measurements in the wake behind the cylinder. These are helpful in the interpretation of such afterglow pictures.

The tests were carried out at stream Mach numbers near two, partly because the flow characteristics of this particular contoured nozzle were well known and partly because at higher Mach numbers flow visualisation using an afterglow technique becomes ineffective due to the higher stagnation pressure of the test gas upstream of the nozzle and the consequent difficulty of causing excitation. Moreover, it was felt that the overall features of supersonic blunt-body flows were not greatly modified by changes in stream Mach number.

The experimental work was done at intervals between October, 1963 and January, 1964.

2. *Experimental Details.*

2.1. *The Tunnel.*

This experiment was carried out in the N.P.L. low-density tunnel, which is described in Ref. 1. A diagram showing the main features of the tunnel is included as Fig. 1 of the present text. The

tunnel is of the continuous-flow open-jet type, powered by oil-vapour booster pumps, suitably backed by mechanical pumps. The free-stream static pressure can be varied between about 10^{-2} mm of Hg (10 microns) and 10^{-1} mm of Hg (100 microns), which represent therefore the limits of the flow pressure range. For the present experiment the tunnel was fitted with a nominal $M_\infty = 2$ nozzle[1]. No heating was applied to the airstream, the stagnation temperature being therefore about room temperature. For convenience, a value of 10°C was adopted in calculating Reynolds number.

The thermistor manometer (described in the Appendix of Ref. 1) was mounted inside the tunnel test chamber and used to record surface pressures on the model. Argon, excited by a R.F. oscillator, was used for flow-visualisation studies about the cylinder.

2.2. *The Models.*

Three basic models (designated A, B and C) were employed. Each model was of cylindrical circular cross-section, with diameters of 0·115 in., 0·25 in. and 0·5 in. (*see* Fig. 3). For the pressure measurements, the cylinders were mounted vertically across the flow supported below the jet by a rotating turntable and, either passing through holes in the plastic extension (or 'skirt') to the solid nozzle (Fig. 2), or held downstream of the exit of the solid nozzle. The smallest model, with only a single pressure hole, had to be rotated through 180° to give a complete circumferential pressure distribution. The two larger models, having more pressure holes, were rotated through 60° to give a complete distribution.

Models A, B and C were designed for pressure-distribution measurements over as wide a range of Reynolds number as possible. A further model (D) was designed to investigate the effect of the pressure-hole size on the recorded pressures.

For flow visualisation, additional non-pressure-plotting models were constructed of wood and mounted horizontally across the flow, supported by the plastic skirt.

2.3. *Test Conditions and Procedure.*

The range of test conditions is given in Table 1. The stream Mach number (M_∞) for all tests was approximately 2, but changes in free-stream static pressure and model size effected the actual value of M_∞. The Reynolds number $(Re_D)_\infty$, based on cylinder diameter (D) and free-stream conditions could be varied both by using the different diameter models and also by variations in the free-stream pressure. The Reynolds number was calculated from Table 1 of Ref. 5, as a function of the free-stream Mach number.

The 0·115 in. and 0·25 in. diameter cylinders were tested inside the plastic extension to the nozzle (*see* Fig. 2). The empty-tunnel Mach number distributions near the model position is given in Ref. 1. The static pressure on the nozzle and test-section wall was measured by means of wall holes in both the skirt and nozzle. The stream total pressure was measured in the settling chamber upstream of the nozzle.

It has been found[1] from previous work in the N.P.L. tunnel that it is essential to run the tunnel with the jet as closely balanced as possible. To achieve this the wall pressure just inside the free end of the nozzle should equal the test-chamber pressure. The effects of even a small degree of out-of-balance pressure extend upstream into the skirt, presumably through the thick wall boundary layer, and by altering the boundary-layer characteristics influence the flow conditions in the test region itself. All results reported here were with either the jet balanced, or for the higher stream pressures as nearly balanced as possible. The size of the small pressure gradients induced at the model position in the latter conditions is discussed in Ref. 1.

A blockage effect associated with the finite model size was encountered when the cylinder models were tested. This showed itself by a change in the wall pressure distribution (from that measured in the empty tunnel) when the model was in position in the test section. Thus the empty-tunnel Mach number distribution could not be used directly to determine the correct free-stream Mach number for the experiment. A direct measurement of the Mach number was made by introducing a 3/8 in. diameter, externally chamfered pitot probe into the flow alongside the cylinder, and making an axial traverse upstream from the cylinder. The Mach number could then be found from the ratio of measured pitot pressure to total pressure. This probe was large enough to have a negligible correction factor due to low Reynolds number effects over the test range of static pressure (*see* Ref.1).

The local Mach number distribution just off axis obtained in this way for the 0·25 in. diameter cylinder is shown in Fig. 4b for various free-stream static pressures. It was felt that the flow to the rear of the model was so strongly influenced by the presence of the 0·25 in. cylinder transverse to the stream that little additional blockage would occur due to the probe. However, the increase in blockage caused by the probe when it was near the 0·115 in. diameter cylinder might not be very small, so that the Mach number distribution obtained for the 0·25 in. cylinder was used for the smaller model also.

Fig. 26 shows that the shock stand-off distance ahead of the cylinder is about one cylinder diameter; hence the free-stream Mach number used in analysing the data was taken to be that just ahead of this position. In an effort to reduce the blockage effect the largest cylinder (0·5 in. diameter) was tested in a free jet, close to the exit plane of the nozzle, with the plastic skirt removed (Fig. 5a). The near-axial Mach number distribution was again measured directly by a 3/8 in. pitot probe alongside the model; results are shown in Fig. 5b. No allowance was made for any small transverse Mach number gradient in the tunnel, since the probe was not far enough off axis for the correction to be significant.

As previously stated, the orifices were placed so that the minimum rotation was required to cover the full 180° from the forward stagnation point to the rear of the model. Each pressure line was connected *via* a pressure outlet on the cylinder top end-face to a separate independent thermistor gauge mounted in a constant-temperature water bath just above the test section (*see* Fig. 2). The range of pressures measured by each gauge was deliberately limited, so that the greatest possible sensitivity could be obtained from each gauge. This technique fitted in well with the fact that for the larger models a given hole had only to scan a small section of the circumference.

The argon-afterglow pictures were taken with a dummy model mounted horizontally across the tunnel, wedged against the walls of the plastic skirt. No model rotation was required. A series of photographs was taken for models of the same diameter as those used for pressure plotting, over a similar range of free-stream pressures. From these pictures estimates of the bow shock stand-off distance and of the wake-flow structure (in argon) could be made.

The 0·5 in. diameter model was used to supplement further the information on wake flow. Pitot-tube traverses, using a 1/8 in. diameter probe, were made in air in the wake behind the cylinder. No corrections were made to the pressures so obtained in order to allow for the low probe Reynolds number, since the general pattern of the wake flow was required, and not particular pressure levels.

For model D, used to obtain information on the influence of pressure-hole size, data were only required in the front region of the cylinder, and a complete circumferential pressure distribution was not taken. Since a direct comparison between the pressures recorded by three different orifices was sought, each orifice was in turn brought to the same angle θ, with as little delay between

readings as possible. This ensured that each orifice measured the same static pressure, assuming that the flow conditions did not change in the short time required to make each set of readings.

It should be noted that in order to locate $\theta = 0$ independently from the scale of the rotating table, the pressure was measured for a range of angles on either side of the indicated zero. The angle for which a maximum pressure was achieved was taken as zero. All subsequent results will be shown using this zero.

3. *Results.*

It is not intended in the present report to give in detail all the results obtained during the experiment. Many of the pressure distributions are similar and it seems more appropriate to present only typical results and then to discuss trends or unusual results which arise. The subsequent discussion may be divided into the following sections.

(1) *Hole-Size Effect.*

This was considered to be of importance in determining the feasibility of using small-diameter pressure holes, and, in particular, of giving information on the best hole size.

(2) *Stagnation-Point Pressure.*

This is also of some importance, since it is possible to compare the circumferential pressure distributions in terms of the ratio of the local pressure coefficient (C_p) to that at the forward stagnation point.

(3) *Circumferential Pressure Distributions.*

In this section the actual pressure distributions will be discussed in terms of the following:

(i) The actual recorded pressure p_θ in microns to show the order of magnitude of the pressures involved and also to illustrate the small experimental scatter present in the pressure measurements.

(ii) Pressure coefficient, C_p, where

$$C_p = \frac{p_\theta - p_\infty}{(\frac{1}{2}\rho U^2)_\infty},$$

and where the various quantities are defined in the List of Symbols.

(iii)

$$\frac{C_p(\theta)}{C_p(0)},$$

the ratio of the local pressure coefficient to that at the stagnation point (i.e. $\theta = 0$). Comparisons can then be made with experimental distributions obtained by other workers.

(4) *Viscous Effects.*

This section deals with the estimation of the viscous effects on the pressure distribution.

(5) *Cylinder Drag.*

The calculation of the cylinder pressure-drag coefficient will be discussed and an estimation of skin friction made using known total-drag coefficients for circular cylinders in low-density flow.

(6) *Flow Model.*

Finally, the general flow pattern about the cylinder may be interpreted using the surface pressure distributions, the information provided by the argon-afterglow photographs and the pitot traverses in the wake.

3.1. *Hole-Size Effect.*

To obtain local pressures, the pressure orifice should be as small as possible. At low densities the actual process by which the pressure outside the orifice is sensed by the measuring gauge *via* the associated tubing is complex. Among other things the measured pressure may well be a function of the orifice diameter (d).

Talbot[9,15] has examined the effect of orifice size on the surface static-pressure readings for slender cones in the slip-flow régime. He found that, as the orifice diameter was increased, so did the apparent pressure. This data was correlated by the equation,

$$\Delta p = 15{\cdot}5\, d\sqrt{M_\infty},$$

where Δp is the pressure increase in microns, M_∞ the free-stream Mach number and d the orifice diameter in inches.

For $M = 2{\cdot}0$ and $d = 0{\cdot}010$ in. this pressure increase is about $0{\cdot}2$ microns. Talbot commented on the fact that for a constant Mach number Δp was insensitive to changes in static pressure, and hence to changes in mean free path. He inferred from this that the orifice-size effect might be a 'ram' effect of the gas into the hole.

Enkenhus[8], on the other hand, working in a very rarefied gas flow using an orifice probe in which the greatest interest was in pressures near the forward stagnation point, found that as the diameter of the orifice was increased, the recorded pressure was reduced; and that no change was observed when the orifice diameter was greater than $0{\cdot}002$ in. (*see* Fig. 6). The orifice probe Enkenhus used consisted of a fine cylindrical metal tube, sealed at one end, with an area of the wall near this end removed. Over this hole was cemented a thin metal foil, $0{\cdot}00031$ in. thick, in which a fine hole was pierced. This difference in hole geometry and local surface inclination probably accounts for the difference between the trend of his results and those obtained by Talbot. The dimensions of hole and pressure tubing of the orifice probe were such that a molecular effusion, or combined molecular effusion and viscous-flow process prevailed.

In the light of these rather divergent results, it was decided to investigate the effect of hole size for the particular geometry and flow régime of the N.P.L. tests. Model D was used for this purpose; this had orifices of diameter $0{\cdot}0020$ in., $0{\cdot}0050$ in. and $0{\cdot}0100$ in. Details of the construction of the pressure holes are shown in Fig. 3. The orifice was actually made in a small bush let into a larger diameter tube, and thus consisted of a tube or 'long' orifice rather than a hole in an infinitely thin wall.

The results of measuring the same pressure with these different orifices is shown in Figs. 6 and 7. The N.P.L. results show the same general trend as Enkenhus' results. The small number of the N.P.L. pressure-hole sizes makes direct comparison rather difficult but it does seem that the curve levels out at a higher value of orifice diameter. It appears that the 'long' orifice should not be less than $0{\cdot}005$ in. in diameter if errors in pressure readings are to be avoided. All subsequent models were constructed to this criterion. Fig. 7 shows that this hole-size effect was largely independent of hole position, at least up to $\theta = 60°$.

3.2. *Stagnation-Point Pressure.*

The pressure in the stagnation region on circular cylinders was investigated by Enkenhus over a wide range of Mach numbers ($0{\cdot}20 \rightarrow 2{\cdot}0$) during the development of the orifice probe*. Some of these data are presented in Fig. 8, in terms of χ, where

$$\chi = \frac{p_{\mathrm{EX}}' - p_{\mathrm{CONT}}'}{p_{\mathrm{FM}}' - p_{\mathrm{CONT}}'}$$

and

$$p' = \frac{p_{\mathrm{stag}}}{p_\infty};$$

the various suffices used are defined in the List of Symbols. The horizontal scale is $M_\infty/(Re_D)_\infty^{1/2}$, where $(Re_D)_\infty$ is a Reynolds number based on free-stream conditions and cylinder diameter. Also shown in this diagram are the values of χ calculated from Tewfik and Giedt's results (Ref. 6) and for the N.P.L. results. p_{CONT}' and p_{FM}' were taken from Ref. 8, both being functions of free-stream Mach number. All the experimental data should be between the limits of $\chi = 0$ and $\chi = 1$, corresponding respectively to continuum and free-molecular flow.

It appears that both the N.P.L. and Enkenhus data are roughly correlated by the parameter $M_\infty/(Re_D)_\infty^{1/2}$ and have similar trends; for comparison the effect of a small Mach number change on χ is shown in the diagram. Some of the scatter may well be due to small errors in the measurement of pressure and Mach number. The differences between the two main sets of results seems real, however, and not easy to explain except in terms of the difference in orifice geometry in the two cases (a 'shallow' orifice with low length/diameter ratio in Ref. 8 and a 'long' orifice in the N.P.L. tests). The three-dimensional effects present in the U.T.I.A. data are probably of small significance. It is interesting to note that appreciable departures from the continuum value of the stagnation-point pressure (i.e. that measured in high Reynolds number flow) exist over the lower part of the present test-pressure range.

3.3. *Circumferential Pressure Distributions.*

Typical surface static-pressure distributions of pressure around a circular cylinder in low-density flow are presented in Fig. 9 in terms of the actual pressure levels. Curve A is for the $0{\cdot}5$ in. diameter cylinder at $M_\infty = 2{\cdot}12$, $(Re_D)_\infty = 134$, while curve B is for the $0{\cdot}115$ in. diameter cylinder with $M_\infty = 1{\cdot}70$, $(Re_D)_\infty = 5{\cdot}4$. These two curves represent distributions for values of Mach number and Reynolds number near the upper and lower limits obtainable in the present tests (*see* Table 1). The pressure is expressed in absolute units to indicate the range and magnitude of pressures encountered during the experiment; the data points define very smooth curves. The subsequent pressure distributions, however, will be presented in terms of the pressure coefficient C_p or by the pressure coefficient rates C_p' (*see* List of Symbols).

The laminar boundary-layer thickness in rarefied flow is approximately proportional to $(Re_x)^{-1/2}$ (Ref. 11). Because a large variation of this parameter was obtained in the present experiment, it is of interest to see the effect of Reynolds number on the pressure distribution. It will be shown later

* These circumferential pressures were measured on a cylinder of finite span at a position relatively close to the tip. No correction can be applied to allow for three-dimensional effects; these are likely to be small, however.

that the pressure distribution is influenced by stream Mach number, so that we need to examine the effect of Reynolds number at constant Mach number.

This has been attempted in Fig. 10, where $M_\infty = 2{\cdot}12$. The actual data points have been omitted for the sake of clarity and because the scatter is very small. It can be seen in this diagram that the effect of increasing Reynolds number is to reduce the pressure coefficient over the entire surface. The previous section showed that the pressure at the forward stagnation point was a function of $M_\infty/(Re_D)_\infty^{1/2}$ which is consistent with the present trend. This difference decreases away from the stagnation point and becomes very small for $60° < \theta < 90°$. Over the rear of the cylinder significant differences again appear.

Calculation of the approximate local Mach number distribution on the surface of the cylinder showed that for $M_\infty = 2{\cdot}15$ the flow was subsonic for θ less than about 40°. It appears from Fig. 10 that it is in this subsonic region that changes of Reynolds number are most significant.

The effect of Mach number is shown in Fig. 11, where the Reynolds number has been held constant at a value of 22. Here it can be seen that there is a general shift in C_p with Mach number, but that the effect is most marked near the stagnation point. As would now be expected in view of earlier discussions, the pressure at the stagnation point increases with Mach number.

It would thus appear, within the range of the parameters encountered in this experiment, that the general pressure coefficient level over the cylinder is influenced by the stream Mach number whilst the detailed shape of the distribution depends more on Reynolds number.

Tewfik and Giedt have also measured the pressure distribution around a circular cylinder at low densities for a range of Mach numbers, including $M_\infty \simeq 2$. These results, however, were for a higher range of Reynolds number (40 to 8 000) than the present experiment. A comparison between Tewfik and Giedt's and the present results is made in Fig. 12, where the stream Mach number for both distributions is 1·90, but where there is a significant difference in Reynolds number. For the region $40° < \theta < 110°$ the two curves are nearly identical. The main differences are for $\theta < 40°$ and towards $\theta = 180°$, differences which are consistent with the influence of Reynolds number discussed earlier.

One rapid, approximate method of estimating the surface pressure distribution is the simple Newtonian-type formula[12, 7]

$$C_p' = \cos^2 \theta \qquad \text{for } (90° \geqslant \theta \geqslant 0°).$$

Comparison between this expression and experiment is shown in Fig. 13; the agreement obtained is not very good in regions away from the neighbourhood of the stagnation point. The Newtonian formula was no more successful when compared with Tewfik's data, and, since this type of approach is reasonably successful in predicting pressures over cylindrical models at higher Reynolds number, a reason for the discrepancy may well be the thick boundary layers present at the low Reynolds numbers. This aspect will be discussed in detail in Section 3.4.

A much more interesting comparison is perhaps shown in Fig. 14. The present results are here compared with a high Reynolds number, continuum-flow pressure distribution[13] at almost the same stream Mach number (1·85). Over the forward part of the cylinder the high Reynolds number results are effectively for inviscid flow, and the differences between these and the N.P.L. results may be regarded as representing the dominant viscous effects. Note that the trend with decreasing Reynolds number shown in Fig. 14 is in the same direction as the departure of the low Reynolds number distribution from the Newtonian-type distribution in Fig. 13. This seems to confirm the explanation for the discrepancy.

3.4. *Viscous Effects.*

It has already been suggested that quite large viscous effects are to be expected due to the presence of thick laminar boundary layers at low Reynolds numbers.

One relatively simple way of estimating the effect of the boundary layer is to use a modified form of the tangent-wedge approximation discussed by Hayes and Probstein[7]. For a two-dimensional body the tangent-wedge theory relates the local surface pressure to that on a wedge whose semi-angle is equal to the local surface inclination of the body to the oncoming flow.

This method has been successfully used in a modified form by Rogers *et al*[1] and others[9,10] for estimating the surface pressure on cones in rarefied supersonic flow. Here a composite body was envisaged consisting of the original body plus its displacement boundary layer. The local surface pressure on the cone was then equated to that on a cone in inviscid flow with the same semi-angle as the local surface inclination of the composite body. This approach could be adapted to the present case by considering the cylinder plus its boundary layer, and fitting an equivalent wedge to the composite body at every point. There are some unsatisfactory features of this flow model and to overcome these the following modification is suggested.

The composite body formed by the cylinder plus its laminar displacement boundary layer is shown in Fig. 15. Consider a point on the surface of the cylinder, say A. The corresponding point on the outer edge of the boundary layer is B, the distance AB is the boundary-layer displacement thickness δ^*. The inclination of the surface to the flow at A is ϕ_A, and that of the boundary layer at B, ϕ_B. The slope of the boundary-layer edge at A is given by

$$\left(\frac{d\delta^*}{dx}\right)_A, \qquad \text{where} \qquad \phi_B - \phi_A = \tan^{-1}\left(\frac{d\delta^*}{dx}\right).$$

Rather than use a wedge of semi-angle ϕ_B to estimate the surface pressure at A, a better estimation would probably be given by equating the pressure at B to some point on a cylinder in inviscid flow where the surface inclination is ϕ_B. This point is the point C on the original cylinder, i.e.

$$\phi_C = \phi_B = \phi_A + \tan^{-1}\left(\frac{d\delta^*}{dx}\right).$$

The proposed method is therefore a 'tangent-cylinder' approximation.

In order to estimate this pressure change the boundary-layer displacement thickness must be calculated. In general methods for making calculations on compressible laminar boundary layers with pressure gradient are very complex. Curle has considered this problem in detail in Ref. 14 and points out that precise numerical solutions for the boundary-layer equations are few, even with the use of high-speed computers, and these only for special cases. Alternative methods which use the actual measured pressure distributions would involve much more computation than is thought practical for this present study.

Ref. 1, however, shows that for a laminar boundary layer on a flat plate with zero heat transfer,

$$\frac{d\delta^*}{dx} \simeq \frac{1{\cdot}73}{2\sqrt{(Re_x)_\infty}}\,(1+0{\cdot}26\,M_L{}^2). \tag{1}$$

Since this expression is for a flat plate, with no allowance made for external pressure gradient, it cannot be expected to give a very accurate value for the displacement thickness slope on a cylinder. Nevertheless, it is a particularly simple expression to apply, and should lead to an order-of-magnitude estimate of $d\delta^*/dx$ if applied well away from the stagnation point. In equation (1), M_L

can be calculated approximately from the ratio $p(\theta)/p(0)$ using isentropic flow tables. The pressure ratio at C on the cylinder, in 'inviscid' flow was taken from the corresponding value of θ in curve 1, Fig. 14. This is the measured pressure distribution[13] on a circular cylinder at $Re \approx 1 \times 10^5$, $M = 1{\cdot}85$.

The results of three such calculations in the region $40° \leqslant \theta \leqslant 100°$ are presented as follows:

(a) Fig. 16: $D = 0{\cdot}25$, $(Re_D)_\infty = 49$, $M_\infty = 2{\cdot}15$,

(b) Fig. 17: $D = 0{\cdot}115$, $(Re_D)_\infty = 34$, $M_\infty = 2{\cdot}08$,

(c) Fig. 18: $D = 0{\cdot}50$, $(Re_D)_\infty = 48$, $M_\infty = 1{\cdot}96$.

It can be seen that the method is quite successful in predicting the experimental distribution for this range of θ, despite the approximations involved. The effect of the thick laminar boundary layer may, therefore, be regarded as reducing the effective θ for a point on the surface upstream of the separation point. The differences between curves 1, 2 and 3 of Fig. 14 can now be explained in terms of this effective change in θ. Because of the progressive reduction in Reynolds number, and hence increasingly thick boundary layers, the pressure given by any angle θ on curves 2 and 3 is given by successively smaller values of θ on curve 1.

3.5. *Cylinder Drag.*

The total drag of cross-stream circular cylinders in the transition régime has been obtained from direct force measurements by Sreekanth[3] at $M \simeq 2{\cdot}0$, and by Maslach and Schaaf[4] at various Mach numbers including a value near 2. Both references quote as an important quantity C_{Dt}, the total-drag coefficient for continuum flow based on previous experimental work in high Reynolds number supersonic flow. C_{Dt} has two components C_{Dp} and C_{Df} which are due to surface normal pressures and tangential shear respectively. The total drag data from Refs. 3 and 4 is summarised in Fig. 19. A smooth curve has been drawn through the experimental data and extrapolated to the continuum-flow limit ($C_{Dt} = 1{\cdot}50$). This curve will be used later to give the total drag of a cylinder in the particular range of Knudsen number (Kn_D) for the present experiment ($0{\cdot}02 < Kn_D < 0{\cdot}5$).

The increase of total drag within the specified range is due to increments in the pressure drag and skin-friction drag; the latter increases rapidly as the Reynolds number is reduced. The pressure drag is modified by changes in the pressure in the separated-flow region to the rear of the model and also by movements of the separation point. Moreover, it has already been shown that the thicker boundary layer associated with the decreasing Reynolds number induces a higher pressure at the same position on the cylinder surface, and this in turn leads to an increase in the pressure-drag coefficient.

The component C_{Dp} for each measured distribution was calculated as follows:

$$C_{Dp} = \frac{\text{(Pressure drag per unit length)}}{(\frac{1}{2}\rho U_\infty^2)_\infty A}$$

where the reference area A is the cross-sectional area per unit length normal to the stream, and hence may be replaced by D. For the complete cylinder,

$$C_{Dp} = \frac{2}{D}\int_0^{\pi D/2} C_p(\theta) \cos\theta \, dx$$

or

$$= \int_0^{\pi} C_p(\theta) \cos\theta \, d\theta .$$

This integral was computed numerically for each pressure distribution. The results are shown in Fig. 20, which represents results for all three cylinders; C_{Dp} is plotted against cylinder Knudsen number. The three sets of data define a smooth curve indicating that C_{Dp} increases gradually with increasing rarefaction. The curve approaches the continuum-flow limit for total drag at the lowest values of Knudsen number, which is only to be expected since the ratio of the continuum-flow skin-friction drag to the total drag is small.

If ΔC_D is defined as the difference:

$$\Delta C_D = C_{Dt} - C_{Dp}$$

then ΔC_D is a measure of the skin-friction drag and is equivalent to C_{Df}. Values of ΔC_D were calculated from the present data for C_{Dp} and from the appropriate value of C_{Dt} taken from Fig. 19. Since the boundary-layer thickness is proportional to $(Re_D)_\infty^{-1/2}$, i.e. $(Kn_D)^{1/2}$*, the calculated values of ΔC_D are plotted against $(Kn_D)^{1/2}$ in Fig. 21. This gives an estimate of the skin-friction drag on the cylinder and this increases almost linearly with $(Kn_D)^{1/2}$. A close approximation to the experimental curve is given by

$$C_{Df} = \frac{1 \cdot 7}{\sqrt{(Re_D)_\infty}}.$$

This is of similar form to the simple expression for the laminar friction-drag coefficient on a flat plate at moderate stream Mach numbers.

3.6. *Flow Model.*

It is difficult to build up a detailed flow model for a circular cylinder in a low-density stream solely from the data obtained in the present tests. Some attempt can be made, however, by exploiting the similarity between some of the present results and those obtained from detailed studies at higher Reynolds number. McCarthy and Kubota[16] have recently reported on the flow characteristics in the wake behind a circular cylinder at $M = 5 \cdot 7$, over a range of Reynolds number between 4 500 to 66 500. Of particular interest is Fig. 10 of this reference (reproduced here as Fig. 23) which is a set of isoaxiometric pitot-pressure traces behind the cylinder in an essentially laminar wake. The results of the present traverses behind the 0·5 in. diameter model shown in Fig. 24 and the overall pattern should be compared with Fig. 23. The wake flow in the present experiment has very similar characteristics, suggesting a laminar wake, like that at the higher Reynolds number of Ref. 16. The trailing-shock system can be identified, and also the 'reverse-flow region' (as designated in Ref. 16) upstream of this system. Another form of presentation of the present wake traverses is shown as Fig. 25, where pitot-pressure isobars are plotted in the field behind the cylinder†. A

---

* Ref. 11 gives

$$Kn = \frac{1 \cdot 26 M \sqrt{\gamma}}{Re}$$

taking $\gamma = 1 \cdot 400$ and $M = 2 \cdot 0$

$$Kn = \frac{2 \cdot 98}{Re}$$

† The pressure levels indicated are those actually recorded in the wake traverse measurements. To give absolute pressure levels (not required in the present argument) these should be corrected for viscous effects. A similar 1/8 in. diameter pitot-tube probe was used in Ref. 1, where the appropriate viscous correction for the probe can be found.

portion of the bow shock can be identified in the region where it enters the nozzle boundary layer, and also the start of a trailing-shock system; both these are indicated on the diagram. The suggested positions of these shocks were confirmed approximately from the argon-afterglow photographs*, but, because the test gas is different in the photographs and in the traverses, a detailed comparison was not possible. Nevertheless, the two shock positions obtained from the two techniques were very similar. These photographs suggested that the trailing-shock system originated well upstream from the 'neck' of the wake.

In Refs. 6 and 16 the pressure distribution over the rear section of the cylinder has been discussed and it is apparent from both experiments that some degree of pressure recovery is encountered in this region. The magnitude of this pressure recovery decreases with decreasing Reynolds number. The point of minimum pressure (which occurs just before the recovery) also moves back toward the rear of the cylinder as the Reynolds number is decreased. This trend was found to continue at the much lower Reynolds numbers of this present experiment, but the magnitude of the pressure recovery is now small. The pressure distribution in the rear region of the cylinders tested is shown in Fig. 22. It can be seen that the recovery is still significant at the highest Reynolds number, but decreases so that it no longer exists at the lowest Reynolds number.

One would expect that this adverse pressure gradient would be associated with separation of the thick boundary layer. Tewfik and Giedt[6] located the separation point at the position of minimum pressure. This probably gives too early a separation in some cases, since the flow could be expected to overcome some adverse pressure gradient. However, this is a convenient criterion for determining approximately the separation point of the laminar boundary layer. At the lowest Reynolds number (5) shown in Fig. 22, the pressure is constant for θ greater than about 160° and thus makes even this simple separation criterion difficult to apply. In general it seems reasonable to locate separation near $\theta = 140°$ for the higher Reynolds numbers, and to suppose that the separation point moves back somewhat with decreasing Reynolds number. By contrast for moderately low Reynolds number flows at very low Mach number, separation occurs near $\theta = 80°$.

A composite diagram, representing the possible flow around the cylinder is shown in Fig. 26. This is based on the matter discussed above, the argon-afterglow photographs and the diagrams of the flow field presented in Ref. 16. It is possible that the details (and perhaps the general geometry) will be different at the lowest Reynolds numbers of the present experiment. Further work at extremely low Reynolds numbers might be of some interest.

The bow-shock stand-off distance was also measured from each of the afterglow photographs. The front of the bow-shock region was taken as the point on the axis in front of the model where the brightness started to increase. This measured distance (ϵ), normalised by dividing by the cylinder diameter (i.e. ϵ/D) is plotted against Reynolds number in Fig. 27. The distances that had to be measured were small, especially for the 0·115 in. diameter cylinder, and this causes some scatter in the data. Nevertheless, it appears that the shock stand-off distance increases as the Reynolds number is decreased. For $(Re_D)_\infty$ greater than about 100 ϵ/D is close to that for high Reynolds number flow. Since both the boundary-layer thickness and shock thickness are not negligible in low-density flow, but are functions of Reynolds number, there will be a particular value of Reynolds

---

* The flow features in the cylinder wake are clearly visible to the eye, but, because of the long exposure time, are less well defined in photographs. The detail would be completely lost if the photographs were reproduced in the present report.

number at which the boundary layer and shock region merge. No indication of the shock thickness was possible from the argon-afterglow pictures, the region between the leading edge of the shock and the body surface being uniformly bright. A rough estimate[15] of the shock thickness (Δs) can be made by assuming that this is 5 mean free-path lengths at the present Mach number. The Knudsen number is by definition the mean free path per diameter, which gives $\Delta s \simeq 15/(Re_D)_\infty$. This is plotted (as $\Delta s/D$) in Fig. 27, and it seems possible to attribute at least some of the movement of the shock stand-off distance to increasing shock thickness.

Similar measurements have been made independently by Bailey and Sims[17]. Here the shock stand-off distance was measured in front of blunt bodies in argon for a Mach number between 4 and 6, and a direct comparison with the present results is not possible. However, the shock detachment distance was found in Ref. 17 to increase with decreasing Reynolds number from the inviscid-flow value. The Reynolds number at which this increase started was about the same for both experiments.

4. *Concluding Remarks.*

The results of the present simple experiment demonstrate the important influence of the thick laminar boundary layer in low Reynolds number flows. On the circular cylinder it would appear that an approximate allowance for the viscous effect on the circumferential pressure distribution can be made by using a 'tangent-cylinder' theory, akin to tangent-wedge methods used for other model geometries. The cylinder pressure distribution is influenced by changes in both the test Reynolds number and Mach number. The latter appears to modify the overall level of the pressure; the former has most effect over the front and rear parts of the cylinder. There is a distinct change in the way the pressure varies over the rear of the model as the Reynolds number is reduced; at the lowest value possible in the present tests[5], the pressure decreases more or less continuously until θ reaches 180°.

These changes in pressure cause the pressure drag to rise with decreasing Reynolds number, and by using earlier measurements of the total drag of cylinders in rarefied gas flow it is possible to deduce how the skin friction varies with Reynolds number. The actual form of the variation is very similar to that for a flat plate with zero heat transfer.

By combining information deduced from argon-afterglow photographs and from pitot traverses to the rear of the cylinder it is possible to show that the wake structure is very similar to that known to exist at high Reynolds number; in particular there was no evidence of a periodic type of flow. Upstream of the model the bow-wave stand-off distance increases as the Reynolds number decreases, and it seems that this change, in part at least, may be related to the increasing shock-wave thickness.

The experiment therefore assists in understanding the nature of low-density flows about aerodynamic shapes, and particularly the part played by the thick laminar boundary layer. Much more work is needed, however, before accurate methods of estimating its effect are available, and the present text should only be regarded as an initial step towards this goal.

LIST OF SYMBOLS

A Reference area

C_{Dt} Total drag coefficient

C_{Df} Skin-friction drag coefficient

C_{Dp} Pressure-drag coefficient

C_p Pressure coefficient $= \dfrac{p_\theta - p_\infty}{(\frac{1}{2}\rho U^2)_\infty}$

$C_{p'} = \dfrac{C_p(\theta)}{C_p(0)}$

d Orifice diameter

D Cylinder diameter

δ^* Boundary-layer displacement thickness

e Bow-shock stand-off distance

Kn Knudsen number $= \dfrac{1{\cdot}485\ M}{Re}$

M Mach number

p Pressure

Re Reynolds number

Δs Shock thickness

θ Angular position, measured from stagnation point

x Distance measured around surface of cylinder

X Axial distance in nozzle

U Velocity

ρ Density

ϕ Inclination of surface to flow

λ Mean free path

$p' = \dfrac{p_{\text{stag}}}{p_\infty}$

$\chi = \dfrac{p_{\text{EX}}' - p_{\text{CONT}}'}{p_{\text{FM}}' - p_{\text{CONT}}'}$

μ Micron (pressure unit; $1\mu = 10^{-3}$ mm of Hg)

LIST OF SYMBOLS—*continued*

Suffices

∞	Free-stream conditions
D	Based on cylinder diameter
EX	Experimental value
FM	Free-molecule value
CONT	Continuum value
stag	Conditions at forward stagnation point
L	Local conditions on surface of cylinder
W	Local conditions at wall of test section
θ	Local conditions at angular position θ
s	Local conditions at separation point

REFERENCES

No.	*Author(s)*	*Title, etc.*
1	E. W. E. Rogers, C. J. Berry and Miss B. M. Davis	Experiments with cones in low-density flows at Mach numbers near 2. N.P.L. Aero. Report 1095. A.R.C. 25 713. March, 1964.
2	H. S. Tsien	Superaerodynamics, Mechanics of rarefied gases. *J. Ae. Sci.*, Vol. 13, p. 653. 1946.
3	A. K. Sreekanth	Drag measurements on circular cylinders and spheres in the transition régime at a Mach number of 2. University of Toronto, U.T.I.A. Report 74. April, 1961.
4	G. J. Maslach and S. A. Schaaf ..	Cylinder drag in the transition from continuum to free molecular flow. University of California, HE–150–194. March, 1962.

REFERENCES—*continued*

No.	*Author(s)*	*Title, etc.*
5	K. R. Enkenhus	The design, instrumentation and operation of the U.T.I.A. low density tunnel. University of Toronto, U.T.I.A. Report 44. June, 1957.
6	O. K. Tewfik and W. H. Giedt ..	Heat transfer, recovery factor and pressure distributions around a cylinder normal to a supersonic rarefied air stream. University of California, Part I. HE–150–162. January, 1959. Part II. HE–150–169. May, 1959.
7	W. D. Hayes and R. F. Probstein	*Hypersonic flow theory.* Academic Press. 1959.
8	K. R. Enkenhus	Pressure probes at very low density. University of Toronto, U.T.I.A. Report 43. January, 1957.
9	L. Talbot, T. Koga and Pauline M. Sherman	Hypersonic viscous flow over slender cones. N.A.C.A. Tech. Note 4327. September, 1958.
10	L. Talbot	Viscosity corrections to cone probes in rarefied supersonic flow at a nominal Mach number of 4. N.A.C.A. Tech. Note 3219. November, 1954.
11	S. A. Schaaf and P. L. Chambré..	*Fundamentals of gas dynamics.* Flow of rarefied gases, Vol. III, Part H of High speed aerodynamics and jet propulsion series. Princeton University Press 1958.
12	L. Lees	Recent developments in hypersonic flow. *Jet Propulsion*, Vol. 27, No. 11, pp. 1162 to 1177. November, 1957.
13	L. Howarth	*Modern developments in fluid dynamics.* High speed flow, Vol. II. Oxford University Press. 1953.
14	N. Curle	*The laminar boundary layer equations.* Chapter 9. Oxford Mathematical Monograph. Oxford University Press. 1962.
15	H. J. Pain and E. W. E. Rogers ..	Shock waves in gases. Reports on Progress in Physics, Vol. XXV, p. 287. The Institute of Physics and the Physical Society. 1962.
16	J. F. McCarthy, Jr. and T. Kubota	A study of wakes behind a circular cylinder at $M = 5{\cdot}7$. A.I.A.A. Summer Meeting, Los Angeles, California, June 17 to 20, 1963, No. 63/170. A.R.C. 25 453. December, 1963.
17	A. B. Bailey and W. H. Sims ..	Shock detachment distance for blunt bodies in argon at low Reynolds number. *A.I.A.A. Journal*, Vol. 1, No. 12, p. 2867. December, 1963.

TABLE 1

Flow Conditions for Experiment

Cylinder Diameter (Inches)	Free-stream Pressure (Microns: 10^{-3} mm of Hg) p_W	Free-stream Mach Number M_∞	Reynolds Number based on Diameter (Free stream) $(Re_D)_\infty$	Reynolds Number based on Diameter (Behind Shock) $(Re_D)_s$	Knudsen Number (Free stream) $Kn = \frac{1 \cdot 485\, M_\infty}{(Re_D)_\infty}$
0 115	20	1·70	5·4	3·9	0·465
	30	1·90	10·3	6·9	0·275
	40	2·06	16·5	10·2	0·186
	50	2·15	22·7	13·4	0·141
	60	2·12	26·4	16·0	0·119
	70	2·10	30·1	18·4	0·104
	80	2·08	33·7	20·8	0·092
0 25	20	1·70	11·8	8·5	0·214
	30	1·90	22·3	15·0	0·126
	40	2·06	35·9	22·2	0·085
	50	2·15	49·4	29·2	0·065
	60	2·12	57·3	34·8	0·055
	70	2·10	65·5	40·0	0·048
	80	2·08	73·2	45·2	0·042
0 50	30	1·96	47·8	31·3	0·061
	50	2·12	95·5	58·0	0·033
	70	2·12	133·7	81·2	0·024

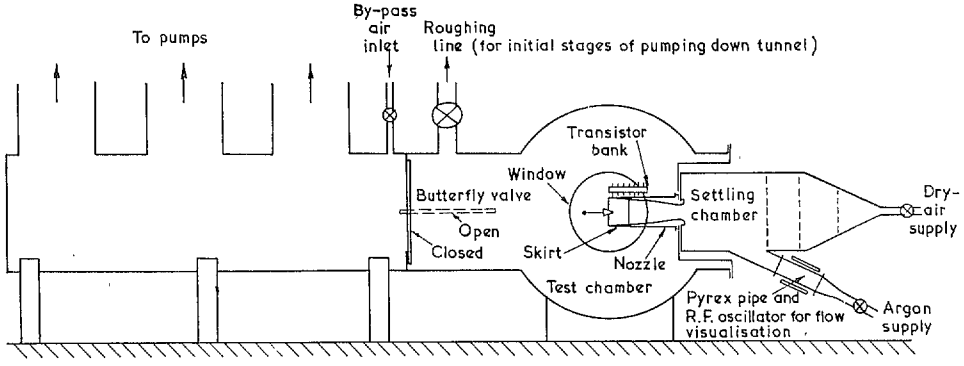

FIG. 1. Diagram of N.P.L. Low Density Tunnel.

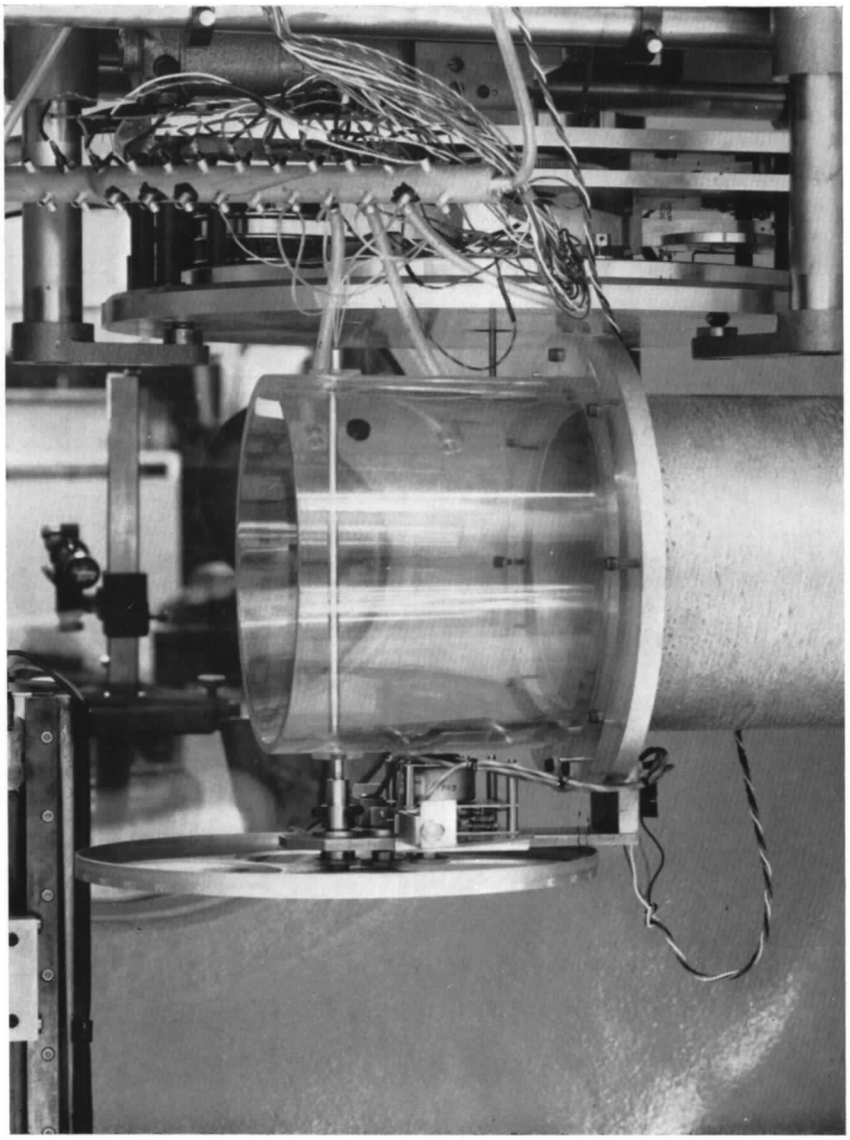

FIG. 2. Photograph of $\frac{1}{4}$ in. diameter model mounted on turn-table and passing through plastic extension to nozzle. The pressure tubes at the upper end of the model are connected to the water-cooled thermistor bank.

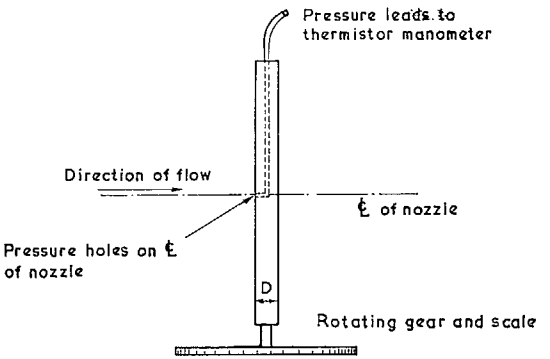

Details of mounting for all models

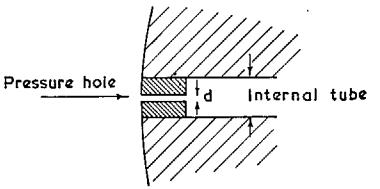

Geometry of pressure measuring hole

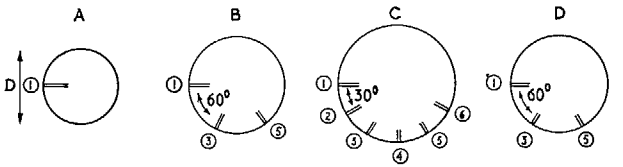

Position of pressure holes

	D	d ①	d ②	d ③	d ④	d ⑤	d ⑥
Model A	0·115″	0·0060″					
Model B	0·250″	0·0054″		0·0060″		0·0060″	
Model C	0·500″	0·0104″	0·0109″	0·0110″	0·0104″	0·0107″	0·0108″
Model D	0·250″	0·0020″		0·0050″		0·0100″	

Dimensions of various cylinders and pressure holes

FIG. 3.

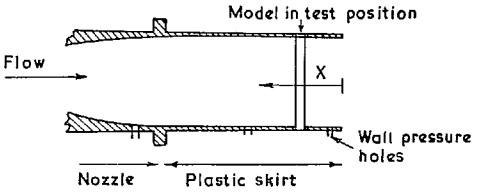

FIG. 4a. Test position for 0·115 in. and 0·25 in. cylinders.

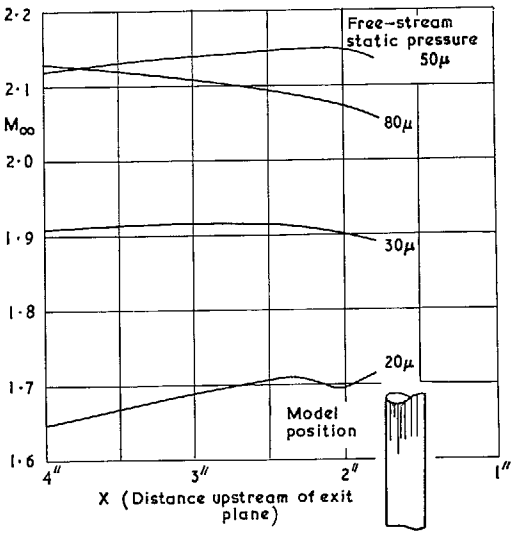

FIG. 4b. Variation in near-axial Mach number distribution as measured with a $\frac{3}{8}$ in. pitot probe with 0·25 in. *D* model in position. (The distribution was assumed to be the same for the 0·115 in. diameter model.)

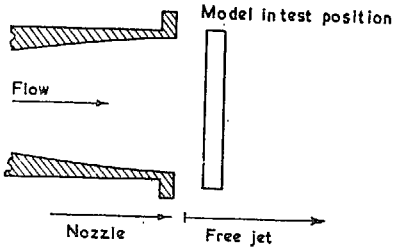

FIG. 5a. Test position for 0·5 in. cylinder.

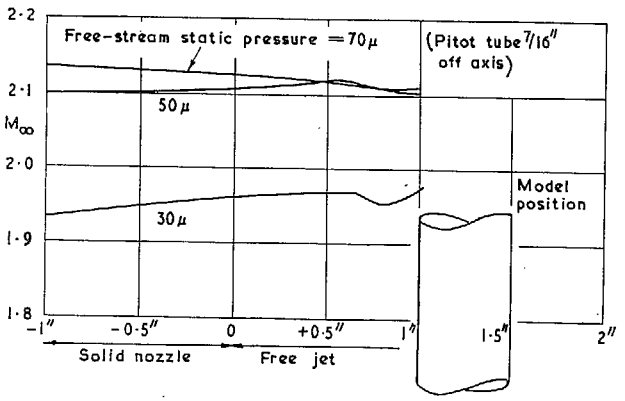

FIG. 5b. Variation with free-stream pressure of near-axial Mach number as measured with $\frac{3}{8}$ in. pitot tube alongside 0·5 in. diameter model.

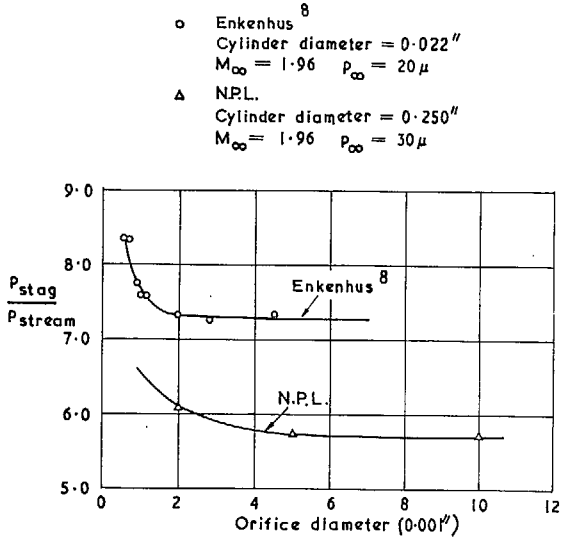

FIG. 6. Comparison of N.P.L. orifice-size effect at $\theta = 0$ with Enkenhus' results.

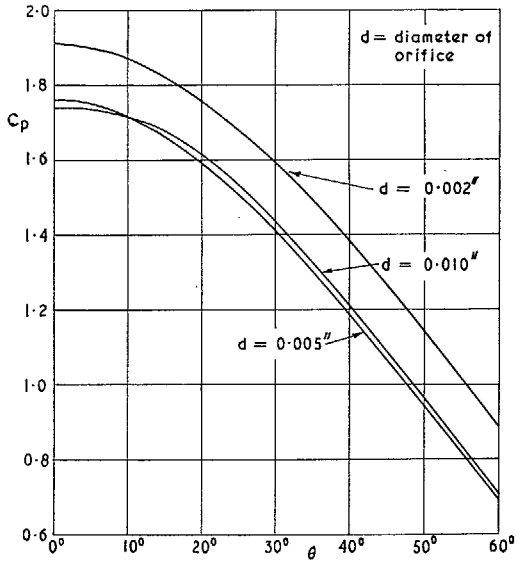

FIG. 7. Effect of orifice diameter on apparent pressure distribution.

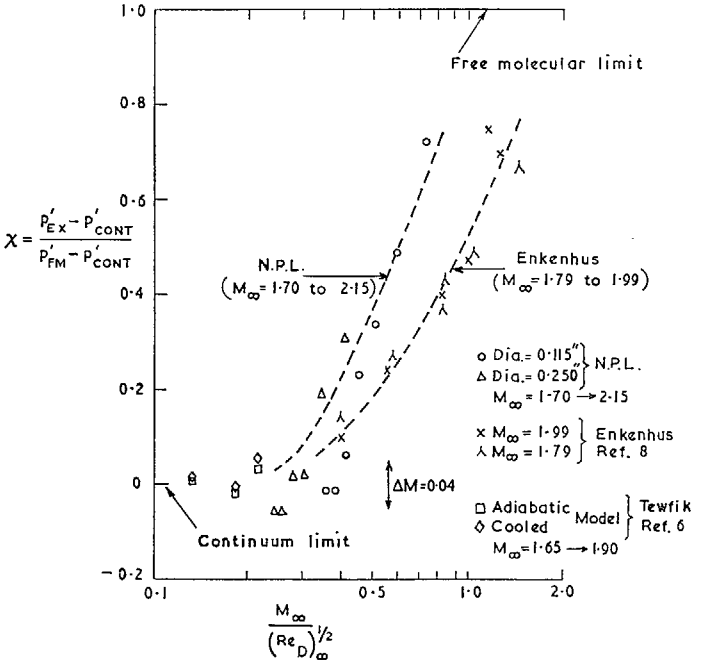

FIG. 8. Forward stagnation-point pressure.

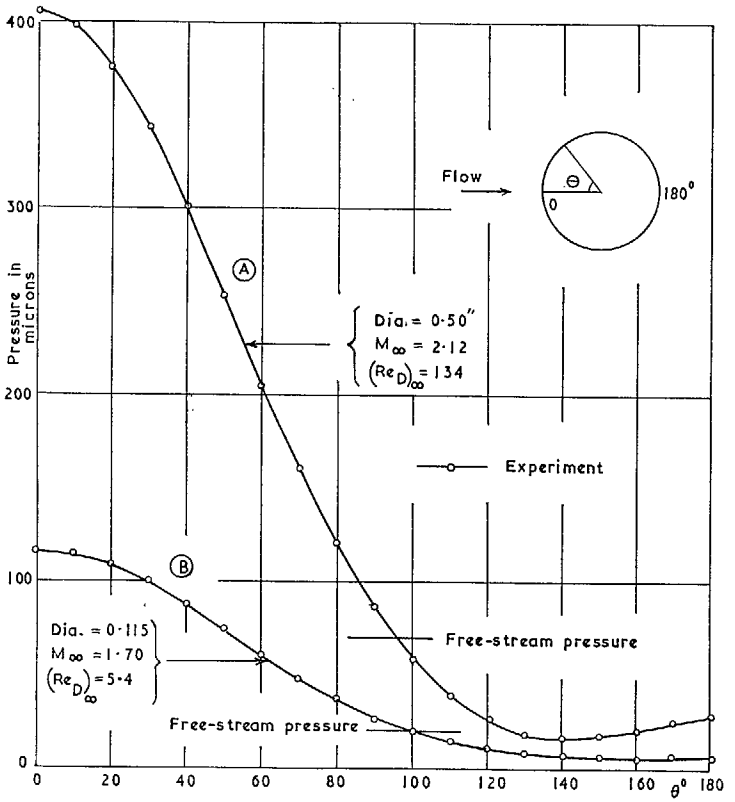

FIG. 9. Pressure distribution around circular cylinder measured in microns (10^{-3} mm of mercury).

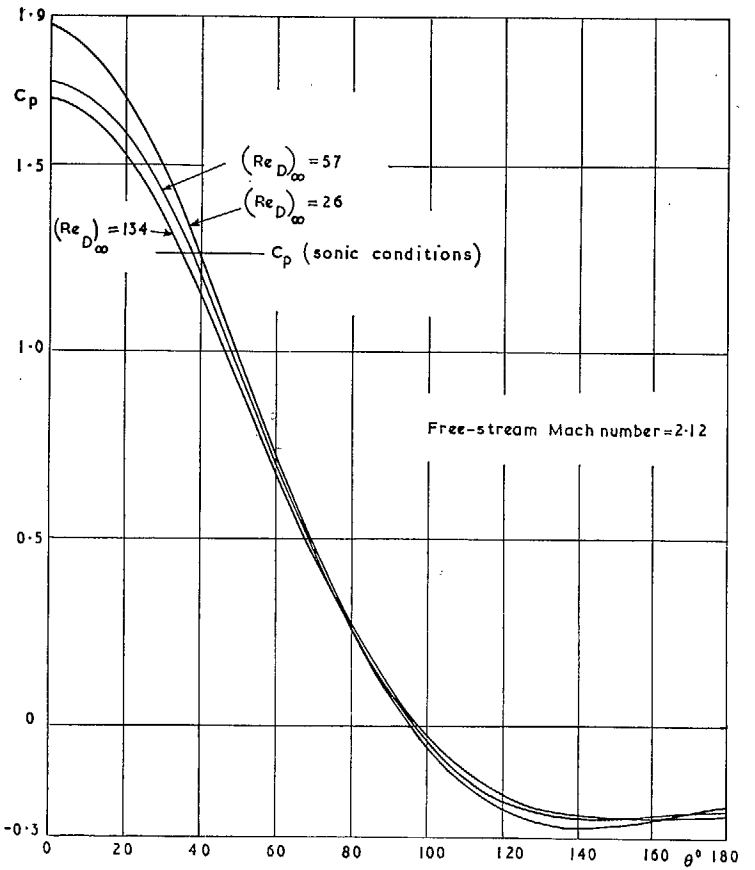

FIG. 10. Effect of Reynolds number on pressure distribution at constant Mach number of 2·12.

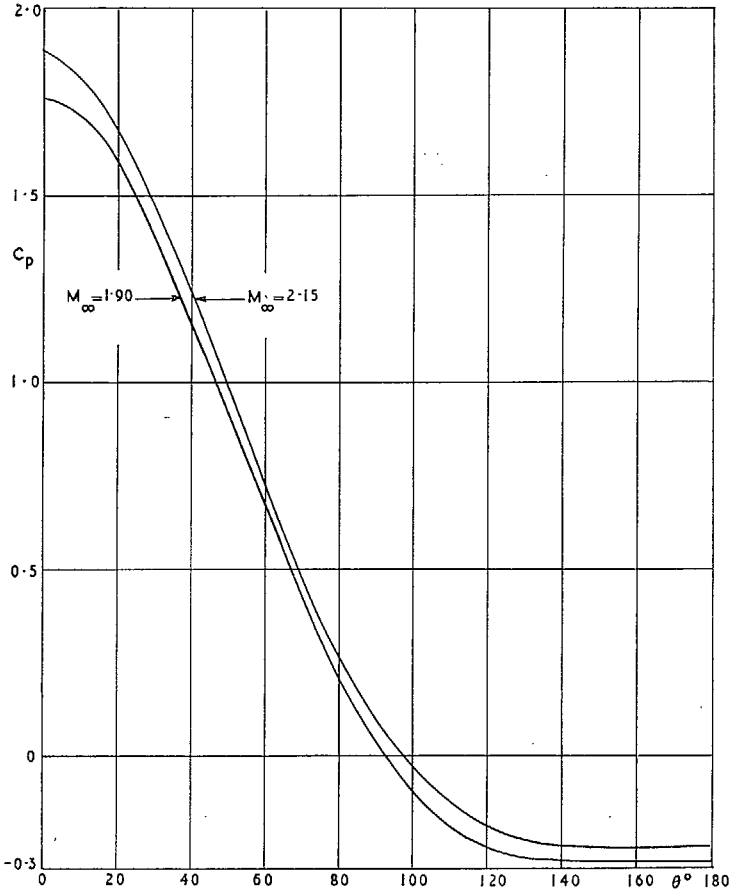

FIG. 11. Effect of stream Mach number on pressure distribution at constant $(Re_D)_\infty = 22$.

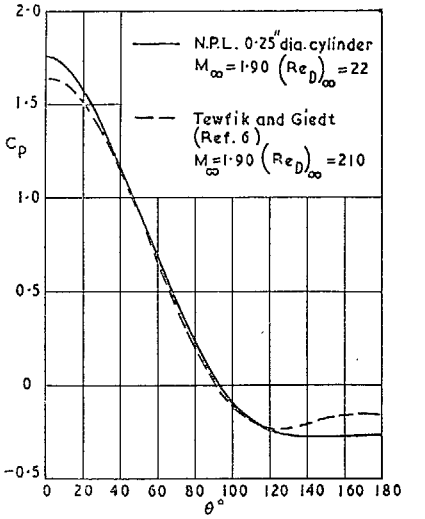

FIG. 12. Comparison between circumferential distribution of C_p obtained by Tewfik and Giedt[6] and that measured in the present experiment.

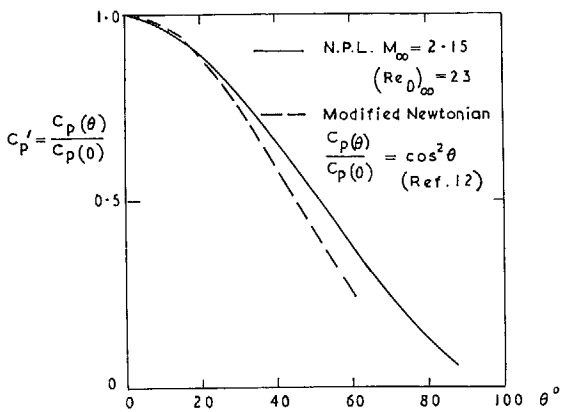

FIG. 13. Comparison of present results with Newtonian pressure law for front section of cylinder.

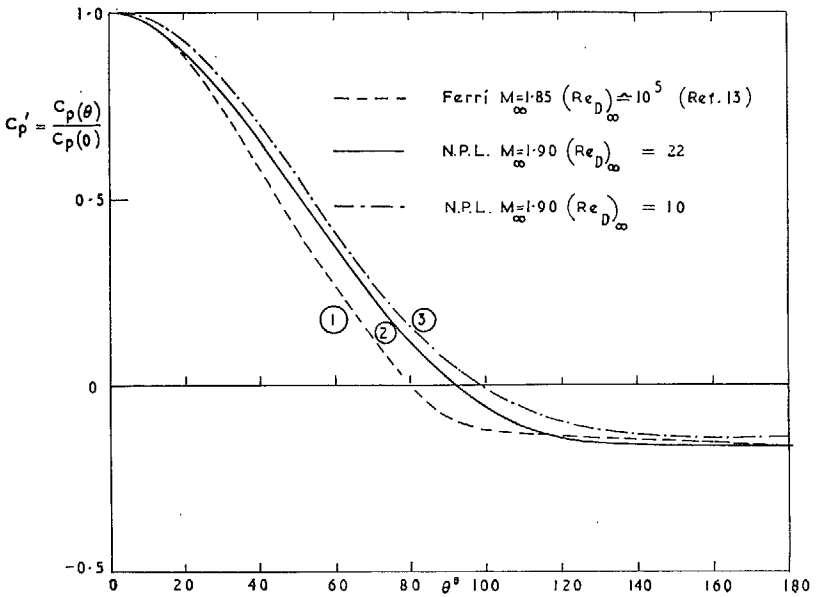

FIG. 14. Comparison of results with high Reynolds number supersonic flow around a cylinder.

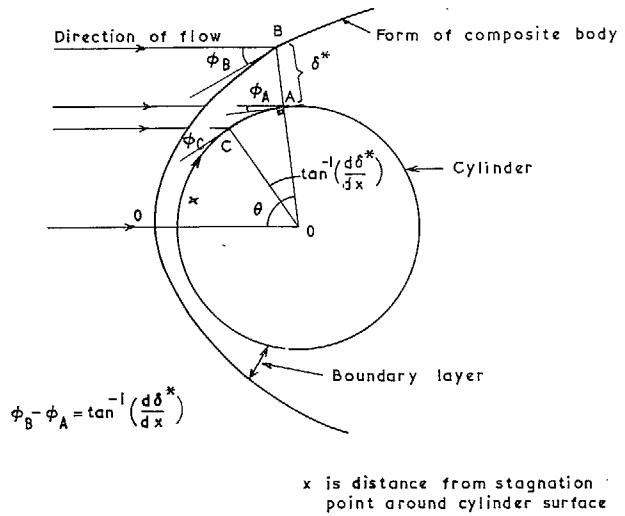

FIG. 15. Notation used in tangent-cylinder approximation.

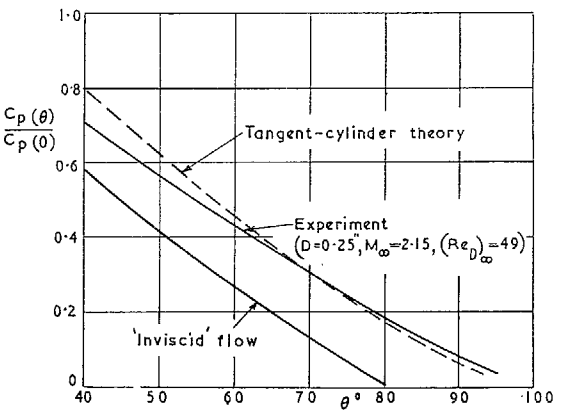

FIG. 16. Prediction of experimental pressure ratios by use of tangent-cylinder theory.

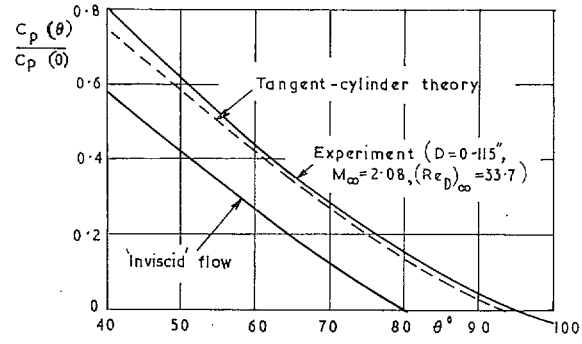

FIG. 17. Prediction of experimental pressure distribution by tangent-cylinder theory.

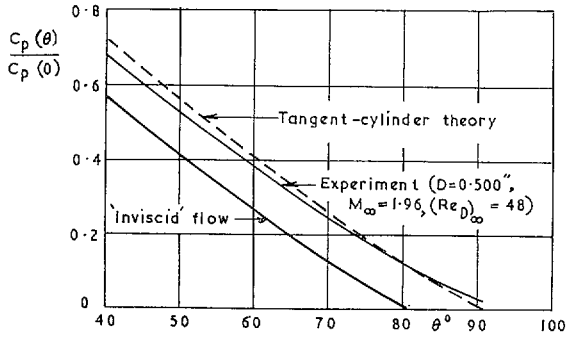

FIG. 18. Prediction of experimental pressure distribution by tangent-cylinder theory.

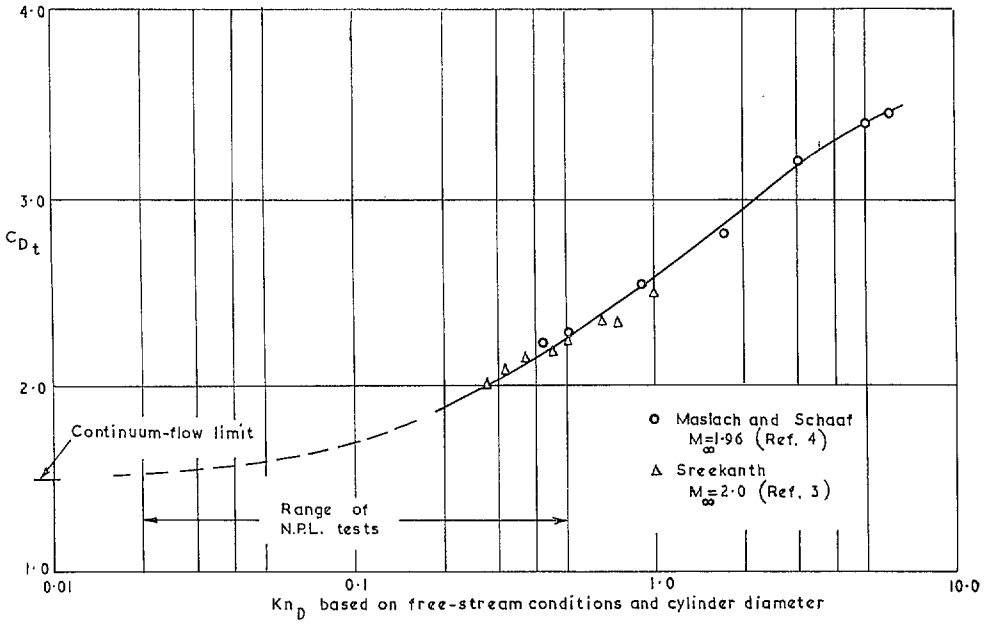

FIG. 19. Total drag on circular cylinder as measured by Maslach and Schaaf[4] ($M_\infty = 1{\cdot}96$) and by Sreekanth[3] ($M_\infty = 2{\cdot}0$).

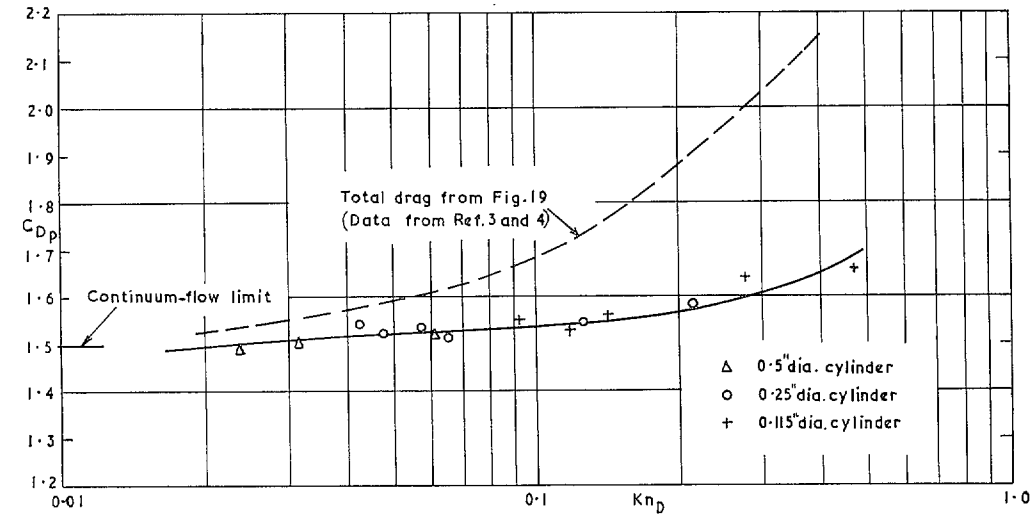

FIG. 20. Calculated pressure drag for the various cylinders of present experiment.

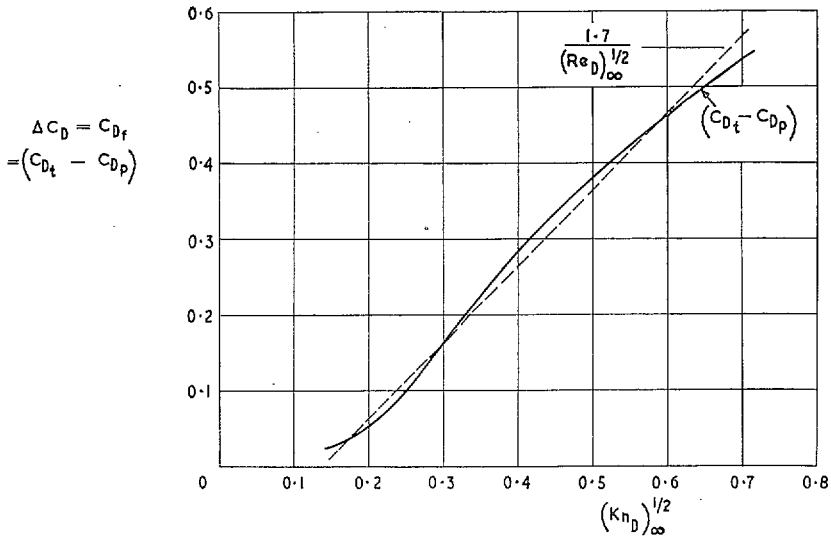

FIG. 21. Estimation of skin-friction contribution to cylinder drag.

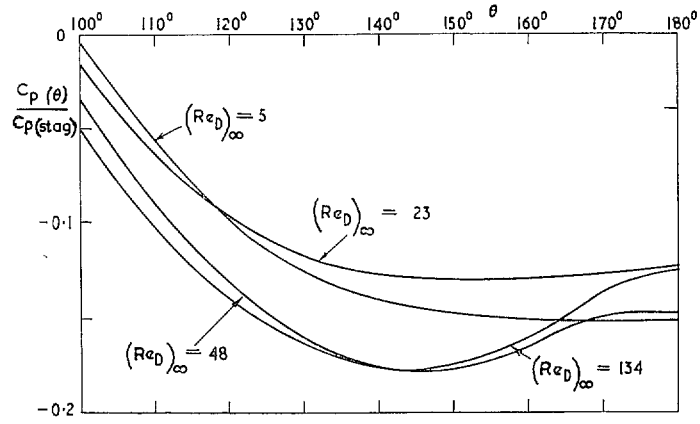

FIG. 22. Pressure distribution near separation point for range of Reynolds number covered by experiment.

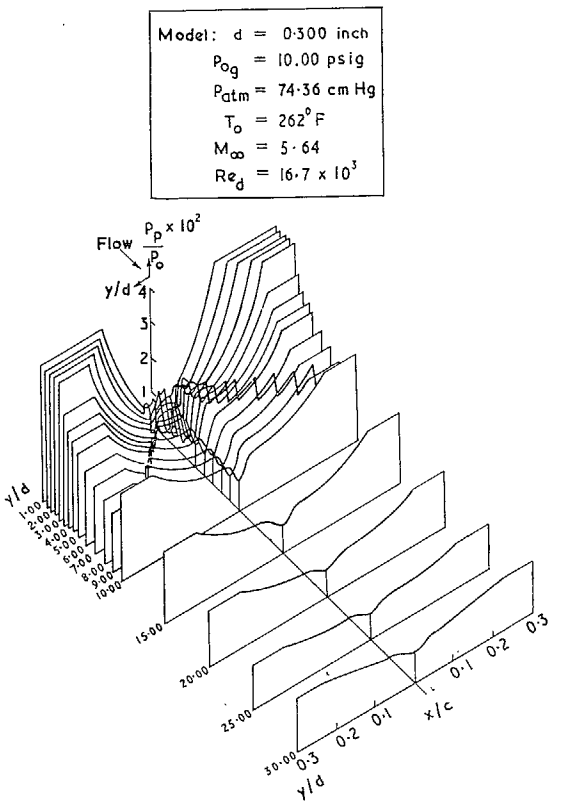

FIG. 23. Total-pressure profiles behind cylinder at $M_\infty = 5{\cdot}64$ (from Ref. 16).

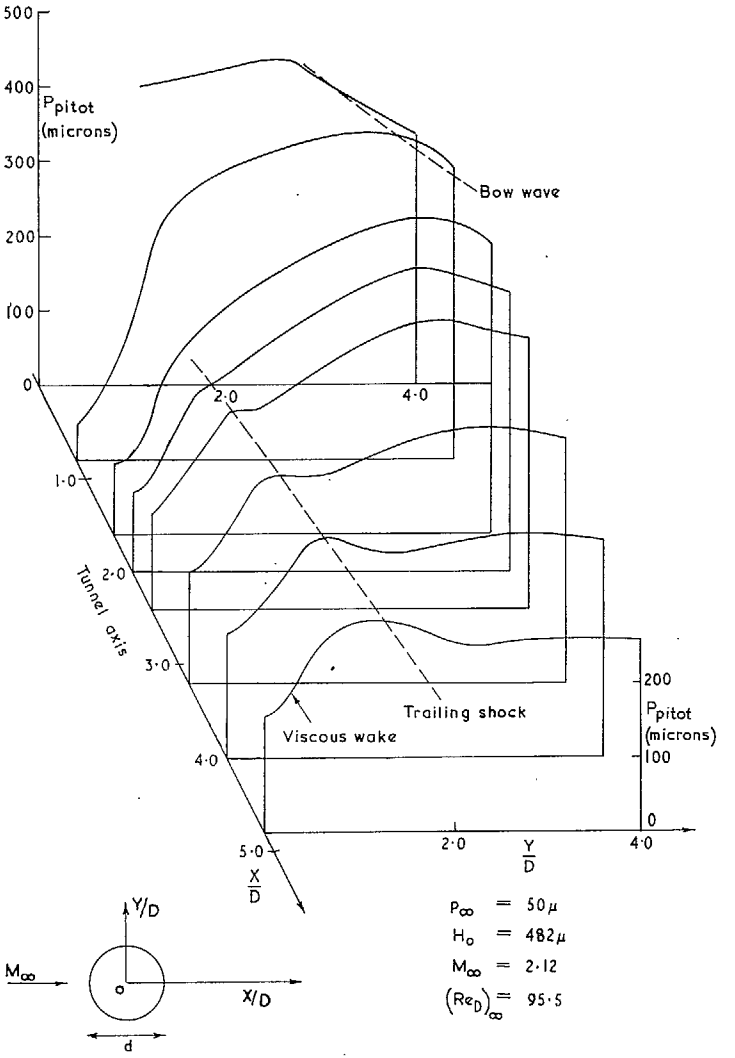

FIG. 24. Total-pressure profiles in wake behind 0·5 in. cylinder (as measured with $\frac{1}{8}$ in. pitot tube).

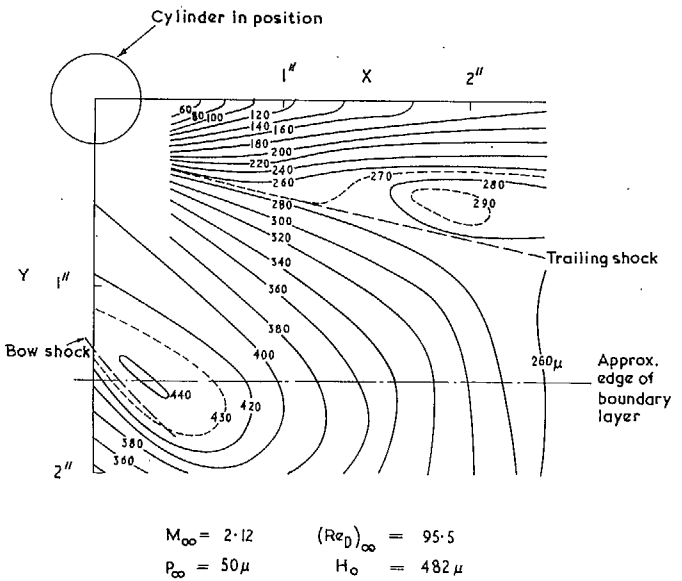

FIG. 25. Pitot-pressure isobars in wake of 0·5 in. diameter cylinder at Reynolds number of 95·5.

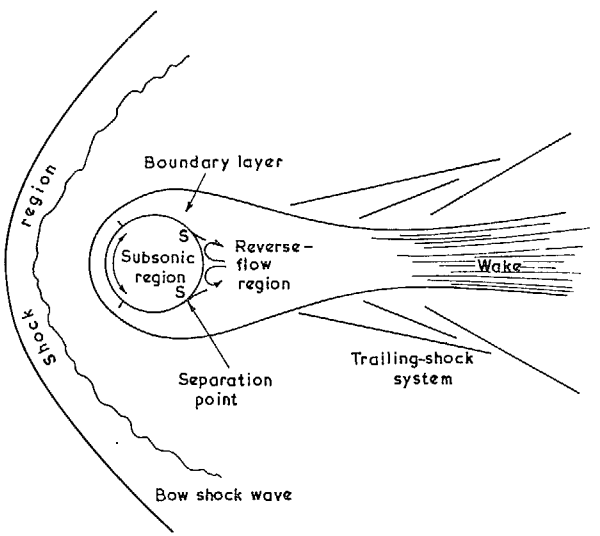

FIG. 26. Suggested flow configuration around circular cylinder at low Reynolds number (based on argon-afterglow photographs, measurements on surface and in wake).

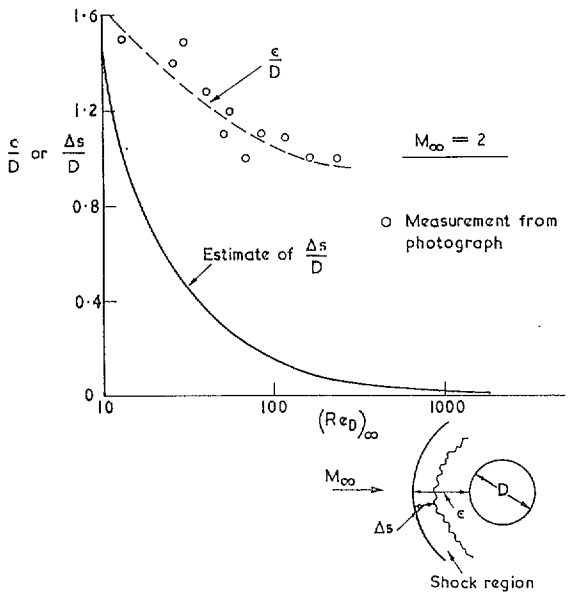

FIG. 27. Variation of measured shock stand-off distance and calculated shock thickness with Reynolds number.

(91678) Wt. 67/2301 K.5 7/65 Hw.

Publications of the Aeronautical Research Council

ANNUAL TECHNICAL REPORTS OF THE AERONAUTICAL RESEARCH COUNCIL (BOUND VOLUMES)

1945 Vol. I. Aero and Hydrodynamics, Aerofoils. £6 10s. (£6 13s. 6d.)
Vol. II. Aircraft, Airscrews, Controls. £6 10s. (£6 13s. 6d.)
Vol. III. Flutter and Vibration, Instruments, Miscellaneous, Parachutes, Plates and Panels, Propulsion. £6 10s. (£6 13s. 6d.)
Vol. IV. Stability, Structures, Wind Tunnels, Wind Tunnel Technique. £6 10s. (£6 13s. 3d.)

1946 Vol. I. Accidents, Aerodynamics, Aerofoils and Hydrofoils. £8 8s. (£8 11s. 9d.)
Vol. II. Airscrews, Cabin Cooling, Chemical Hazards, Controls, Flames, Flutter, Helicopters, Instruments and Instrumentation, Interference, Jets, Miscellaneous, Parachutes. £8 8s. (£8 11s. 3d.)
Vol. III. Performance, Propulsion, Seaplanes, Stability, Structures, Wind Tunnels. £8 8s. (£8 11s. 6d.)

1947 Vol. I. Aerodynamics, Aerofoils, Aircraft. £8 8s. (£8 11s. 9d.)
Vol. II. Airscrews and Rotors, Controls, Flutter, Materials, Miscellaneous, Parachutes, Propulsion, Seaplanes, Stability, Structures, Take-off and Landing. £8 8s. (£8 11s. 9d.)

1948 Vol. I. Aerodynamics, Aerofoils, Aircraft, Airscrews, Controls, Flutter and Vibration, Helicopters, Instruments, Propulsion, Seaplane, Stability, Structures, Wind Tunnels. £6 10s. (£6 13s. 3d.)
Vol. II. Aerodynamics, Aerofoils, Aircraft, Airscrews, Controls, Flutter and Vibration, Helicopters, Instruments, Propulsion, Seaplane, Stability, Structures, Wind Tunnels. £5 10s. (£5 13s. 3d.)

1949 Vol. I. Aerodynamics, Aerofoils. £5 10s. (£5 13s. 3d.)
Vol. II. Aircraft, Controls, Flutter and Vibration, Helicopters, Instruments, Materials, Seaplanes, Structures, Wind Tunnels. £5 10s. (£5 13s.)

1950 Vol. I. Aerodynamics, Aerofoils, Aircraft. £5 12s. 6d. (£5 16s.)
Vol. II. Apparatus, Flutter and Vibration, Meteorology, Panels, Performance, Rotorcraft, Seaplanes. £4 (£4 3s.)
Vol. III. Stability and Control, Structures, Thermodynamics, Visual Aids, Wind Tunnels. £4 (£4 2s. 9d.)

1951 Vol. I. Aerodynamics, Aerofoils. £6 10s. (£6 13s. 3d.)
Vol. II. Compressors and Turbines, Flutter, Instruments, Mathematics, Ropes, Rotorcraft, Stability and Control, Structures, Wind Tunnels. £5 10s. (£5 13s. 3d.)

1952 Vol. I. Aerodynamics, Aerofoils. £8 8s. (£8 11s. 3d.)
Vol. II. Aircraft, Bodies, Compressors, Controls, Equipment, Flutter and Oscillation, Rotorcraft, Seaplanes, Structures. £5 10s. (£5 13s.)

1953 Vol. I. Aerodynamics, Aerofoils and Wings, Aircraft, Compressors and Turbines, Controls. £6 (£6 3s. 3d.)
Vol. II. Flutter and Oscillation, Gusts, Helicopters, Performance, Seaplanes, Stability, Structures, Thermodynamics, Turbulence. £5 5s. (£5 8s. 3d.)

1954 Aero and Hydrodynamics, Aerofoils, Arrester gear, Compressors and Turbines, Flutter, Materials, Performance, Rotorcraft, Stability and Control, Structures. £7 7s. (£7 10s. 6d.)

Special Volumes

Vol. I. Aero and Hydrodynamics, Aerofoils, Controls, Flutter, Kites, Parachutes, Performance, Propulsion, Stability. £6 6s. (£6 9s.)
Vol. II. Aero and Hydrodynamics, Aerofoils, Airscrews, Controls, Flutter, Materials, Miscellaneous, Parachutes, Propulsion, Stability, Structures. £7 7s. (£7 10s.)
Vol. III. Aero and Hydrodynamics, Aerofoils, Airscrews, Controls, Flutter, Kites, Miscellaneous, Parachutes, Propulsion, Seaplanes, Stability, Structures, Test Equipment. £9 9s. (£9 12s. 9d.)

Reviews of the Aeronautical Research Council

1949–54 5s. (5s. 5d.)

Index to all Reports and Memoranda published in the Annual Technical Reports

1909–1947 R. & M. 2600 (out of print)

Indexes to the Reports and Memoranda of the Aeronautical Research Council

Between Nos. 2451–2549: R. & M. No. 2550 2s. 6d. (2s. 9d.); Between Nos. 2651–2749: R. & M. No. 2750 2s. 6d. (2s. 9d.); Between Nos. 2751–2849: R. & M. No. 2850 2s. 6d. (2s. 9d.); Between Nos. 2851–2949: R. & M. No. 2950 3s. (3s. 3d.); Between Nos. 2951–3049: R. & M. No. 3050 3s. 6d. (3s. 9d.); Between Nos. 3051–3149: R. & M. No. 3150 3s. 6d. (3s. 9d.); Between Nos. 3151–3249: R. & M. No. 3250 3s. 6d. (3s. 9d.); Between Nos. 3251–3349: R. & M. No. 3350 3s. 6d. (3s. 10d.)

Prices in brackets include postage

Government publications can be purchased over the counter or by post from the Government Bookshops in London, Edinburgh, Cardiff, Belfast, Manchester, Birmingham and Bristol, or through any bookseller

Printed and published by
HER MAJESTY'S STATIONERY OFFICE

To be purchased from
York House, Kingsway, London W.C.2
423 Oxford Street, London W.1
13A Castle Street, Edinburgh 2
109 St. Mary Street, Cardiff
39 King Street, Manchester 2
50 Fairfax Street, Bristol 1
35 Smallbrook, Ringway, Birmingham 5
80 Chichester Street, Belfast 1
or through any bookseller

Printed in England

R. & M. No. 3416

S.O. Code No. 23-3416